Dichotomy of metallic electron density and charge density wave in $1T$-$TiSe_2$

Dongjoon Jeong [1,2] Jimin Kim [1] Kyung-Hwan Jin [1] Jaeyoung Kim,[1] and Han Woong Yeom [1,2,*]
[1]*Center for Artificial Low Dimensional Electronic Systems, Institute for Basic Science (IBS), Pohang 37673, Republic of Korea*
[2]*Department of Physics, Pohang University of Science and Technology (POSTECH), Pohang 37673, Republic of Korea*

(Received 21 October 2023; revised 3 January 2024; accepted 20 February 2024; published 11 March 2024)

$1T$-$TiSe_2$ has been intensely investigated for its intriguing charge density wave (CDW) phase, which competes with emerging superconductivity. However, the mechanism of the CDW transition has been elusive with the possibility of strong excitonic interaction. Here, we investigate, using angle-resolved photoelectron spectroscopy and density functional theory calculations, the evolution of the CDW band structure upon electron doping into the surface layer by alkali metal adsorbates. Alkali metal adsorption induces substantial electron donation into the Ti $3d$ conduction band with strong band renormalization while the Se $4p$ valance band is contrastingly intact. The density functional theory calculations reveal that only the spectator-type Ti $3d$ band is selectively doped with the CDW band gap largely intact. This result indicates that the CDW formation is not critically related to the metallic electron density and, in turn, to the excitonic coupling due to its unique multiband configuration.

DOI: 10.1103/PhysRevB.109.125117

I. INTRODUCTION

Electronic properties of layered van der Waals materials such as transition-metal dichalcogenides (TMDC) [1] are attracting a great deal of fundamental and technological interest. In particular, $1T$ polytype metallic TMDC materials [Fig. 1(a)] usually fall into charge density wave (CDW) phases, which are entangled with various many-body quantum states such as Mott insulators and quantum-spin liquids (for a well known example, $1T$-TaS_2 [2,3]), excitonic insulators ($1T$-$TiSe_2$ [4–7]), or emerging superconductivity (for both $1T$-TaS_2 [8–10] and $1T$-$TiSe_2$ [11–13]). The nature of these many-body ground states with both strong Coulomb interactions and electron-phonon interaction has not been clear for bulk crystals even after decades of investigations as well as for monolayer systems fabricated recently.

In the case of the CDW phase of $1T$-$TiSe_2$, the origin of the CDW transition has been debated between mainly phononic and excitonic mechanisms. This material is indeed a unique case of CDW, which has been discussed in relationship with the spontaneous formation of excitons. It hosts $2a \times 2b \times 2c$ commensurate CDW at $T_c = 202$ K [14], which turns into a superconducting state when suppressed by Cu intercalation [11], pressure [12], and electric field [13]. Early studies suggested the Fermi-surface-nesting mechanism connecting the Se $4p$ valence band at Γ point and the partially occupied Ti $3d$ conduction band at L point [15]. However, no significant nesting in the Fermi surfaces was identified. Later works discussed the band-type Jahn-Teller effect [16–18] and the excitonic insulator scenario [4–7]. Experimental indications of both strong electron-lattice interaction [19,20] and the plasmonic interaction, which can be related to the exciton formation [5,21,22], have been accumulated and prevented to pin down the major driving force of the phase transition.

However, a recent electron energy loss spectroscopy study showed the detailed temperature evolution of the plasmonic mode [23], which rules out the plasmon softening proposed in an earlier study, the major experimental ground for the existence of the excitonic interaction. While this updated finding seems to deny the strong excitonic contribution to the transition, a very recent angle-resolved photoelectron spectroscopy (ARPES) study suggested that a major part of the band gap is collapsed by the surface electron doping and attributed this gap to the exciton condensation [24].

In the present work, we reinvestigate the evolution of the band dispersions of $1T$-$TiSe_2$ upon the surface electron doping using ARPES under alkali metal adsorption and density functional theory (DFT) calculations. We find that only one Ti $3d$ conduction band, among a few, of the topmost layer selectively takes electrons from K adsorbates and undergoes strong renormalization of its dispersion. In clear contrast, Se $4p$ valence band exhibits no substantial change with only a marginal energy shift. The DFT calculation reproduces those unusual changes in the band structure, revealing the selective electron doping into the spectator-type Ti $3d$ band, which is not actively involved in the CDW formation. The band-selective doping leaves the CDW-related bands largely intact even under a huge amount of metallic electrons. This unusual doping behavior and the separation of metallic electrons from the CDW formation indicates that the excitonic coupling, being sensitive to the screening, is not crucial. Instead, the overall band restructuring upon surface doping fits well with the band-type Jahn-Teller mechanism. The multiband configuration of the conduction band plays a unique role in the formation of the CDW and its response to electron doping. This work implies that superconductivity and the CDW are not necessarily coupled nor do they compete in the present system.

II. METHODS

We used commercial $1T$-$TiSe_2$ crystals (HQ graphene), whose quality was checked by Raman spectroscopy, x-ray

*yeom@postech.ac.kr

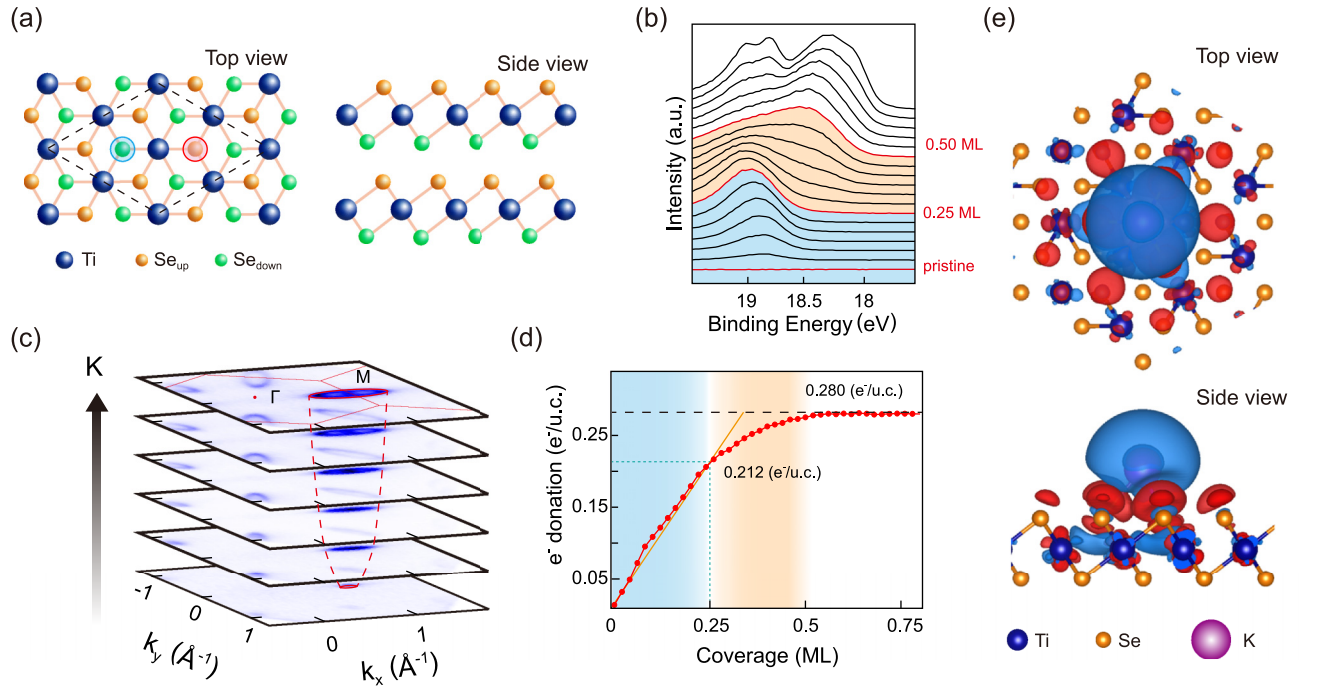

FIG. 1. (a) Top and side view of the atomic structure of undistorted $1T$-$TiSe_2$.The dashed lines indicate a 2×2 CDW unitcell. The blue (red) circle indicates the favored (the second favored) K adsorption site determined by DFT calculations. (b) Evolution of K $3p$ photoelectron spectra during the continuous K deposition. (c) Evolution of the Fermi surface measured at $T = 77$ K with a photon energy of 100 eV during the K deposition. The bottom layer shows the spectrum of the pristine sample and the top one with K of 0.25 ML. (d) The amount of electron donation at different K coverages as estimated by the size of the Fermi surface through the Luttinger theorem. (e) Top and side views of isosurfaces of charge density changes (accumulation and depletion in red and blue colors, respectively) after the K adsorption on $1T$-$TiSe_2$. Electrons from the K adatom are transferred to the substrate and the energy level of its $4s$ orbital is located within the range of 1–2 eV above the Fermi level.

diffraction, and energy-dispersive x-ray spectroscopy. Horizontally polarized photon beams from an undulator beamline (4A2) of Pohang Light Source and another undulator beamline (4.0.3) of Advanced Light Source were used for the ARPES measurements. We chose 100 and 78 eV as the incident photon energy, which are optimized to measure the ΓM and AL direction [25] of the Brillouin zone (BZ), where the CDW-related features are most clearly resolved due to the k_z-selective interband hybridization (Fig. S1 in Ref. [26]) [25]. The samples were cleaved in ultra-high vacuum for ARPES experiments, which were performed at temperatures of 77 K (at Pohang Light Source) and 10 K (at Advanced Light Source) under a constant K flux from effusion cells. The energy and angular resolution were better than 20 meV and 0.1°, respectively.

Electronic structure calculations were performed within the framework of DFT using the Perdew-Burke-Ernzerhof-type generalized gradient approximation for the exchange-correlation functional, as implemented in the Vienna *ab initio* simulation package [27,28]. A K-adsorbed $TiSe_2$ surface has been modeled using a 2×2 supercell with a K adlayer of 0.25 ML, one K adatom in each supercell. The choice of this particular coverage is made clear below. The substrate consists of a double-layer slab [Fig. 1(a)], which is a minimal structural unit in the $2 \times 2 \times 2$ CDW structure. One bilayer unit is sufficient to effectively describe the electronic structure of the K adsorption, since the electron transfer is highly localized to the topmost layer leaving the electronic states of layers underneath almost intact (see Fig. S2 in Ref. [26]). In order to incorporate the chirality, the CDW structure is constructed from the lowest-energy bulk structure with a space group C_2 symmetry [29], which has a consistent in-plane structure with the prevailing structure model of the $P\bar{3}c1$ symmetry but has a different layer stacking for the bilayer. However, there is not a significant difference in the calculated band dispersions between the C_2 and $P\bar{3}c1$ structure models (Fig. S3 in Ref. [26]). We used a vacuum region of 20 Å to avoid interaction between periodically repeated slabs. All calculations were carried out using the kinetic energy cutoff of 520 eV on a $11 \times 11 \times 1$ Monkhorst-Pack k-point mesh. Lattice parameters and ionic positions were optimized until the residual force on each ion was less than 0.01 eV $Å^{-1}$. The electronic self-consistent iteration was converged to 10^{-5} eV precision of the total energy. The spin-orbit coupling is included within the self-consistent calculation. The amount of doped electrons from the K layer can be artificially controlled by changing the distance between K and $1T$-$TiSe_2$ layers.

III. RESULTS AND DISCUSSION

Before discussing the detailed electronic band structure, we first characterize the adsorption behavior of alkali metal K on $1T$-$TiSe_2$. Figure 1(b) shows the evolution of K $3p$ core-level photoelectron spectra during the continuous

deposition of K atoms on $1T$-$TiSe_2$ at 10 K. The K coverage of each spectrum is calibrated by the total area of spectral peaks and the photoionization crosssection. The intercalation of K inbetween layers is not considered since no such signature is observed in K $3p$ core-level spectra and the energy barrier for the direct intercalation of alkali metal in $TiSe_2$ is too high to overcome at low temperature [30]. Here, one monolayer (ML) is defined by the coverage where every 1×1 surface unitcell is occupied by a single K adatom, so each 2×2 CDW unit cell contains one K atom at 0.25 ML. The recent scanning tunneling miscroscopy study showed that K adatoms are well dispersed and respect the 2×2 CDW superstructure below 0.25 ML [31]. At the initial stage of the adsorption, one $3p$ component at a binding energy of 18.8 eV dominates. However, this component saturates above 0.25 ML and the second component at a lower binding energy of 18.3 eV starts to grow. That is, there exist two different adsorption sites, which appear in distinct coverage regimes [Fig. 1(b)] up to about 0.5 ML. This behavior is simple to understand since the transition coverage between these adsorption sites is close to 0.25 ML, a single adatom on each 2×2 CDW unit cell. That is, each CDW unit cell is occupied by a single K adatom in a unique site until these sites are depleted and then an extra site starts to be occupied. As the other possibility, the initial and the second stage can just represent the 2×2 CDW unit cells singlely and doubly occupied by K adsorbates, respectively. A significantly higher binding energy of the first site can then be due to the energy difference of two distinct adsorption sites or the singlely and doubly occupied cases. Beyond 0.5 ML, more than two adatoms within a 2×2 CDW unit cell, several extra $3p$ components appear. It is straightforward that K starts to adsorb in multiple sites. This indicates that the first K adlayer, which actively interacts with the $1T$-$TiSe_2$ surface layer, completes at around 0.5 ML with two K atoms within each CDW unit cell. Our discussion below, thus, focuses on the first two phase of the adsorption up to 0.5 ML, where the occupation of two well-defined sites per 2×2 CDW unit cell occurs in two distinct stages [Blue and red sites in Figs. 1(a) and 1(b). See the discussion below].

In this coverage range, the surface layer becomes metallic and the electron occupation increases monotonically as monitored by the appearance and the size of the electron pocket at the Fermi energy [Fig. 1(c)]. This change is naturally interpreted as due to the electron donation from K adatoms to the $1T$-$TiSe_2$ surface layer. This interpretation will further be supported by the DFT calculation below. The Luttinger theorem can quantitatively estimate the electron density donated; the number of carriers is defined as $n = 2\frac{VV_{FS}}{(2\pi)^d}$, where V is the volume of the system unit cell, V_{FS} the volume of the Fermi surface, and d the dimension of the system 3 [32]. The electron density estimated as such increases almost linearly up to the coverage of 0.25 ML, the depletion of the initial sites, but grows with a much slower rate over 0.25 ML up to the saturation at around 0.5 ML [Fig. 1(d)]. These data provide a clear picture of the charge-transfer interaction between the K layer and the surface layer [Fig. 1(e)]; about 0.21 electron/unitcell is donated by a single K adsorbate in its favored site, which decreases for the second adsorption sites above 0.25 ML. No further electron doping occurs beyond 0.5 ML. This agrees well with the picture provided by the evolution of K $3p$ core level spectra.

We then track ARPES valence-band maps during the continuous deposition of K up to 0.5 ML at 10 K, which is well below the CDW transition temperature. Figure 2(a) shows the evolution of the band structure at the M point on which the electron pocket shown in Fig. 1(c) is centered. It is well known that the lowest Ti $3d$ conduction band (C^1 band in the figure) in the CDW state is partially occupied around the L point (78 eV in photon energy) with an elliptical electron pocket [Fig. 1(c)] but located above the Fermi level at the M point (100 eV photon energy) [25]. Its bottom at L (M) constitutes the apparent band gap of 120 (220) meV together with the top of the Se $4p$ valence bands (V band). The latter is folded from the Γ point due to the CDW superstructure, and its intensity decreases for the increase of the temperature or the inclusion of disorder [33–35]. That is, its intensity at M correlates with the CDW order. Upon the alkali metal adsorption, the band dispersions near the Fermi energy evolve drastically within the first and second phases of the adsorption in Fig. 1(b) up to 0.5 ML and saturates in the third adsorption regime beyond 0.5 ML (Fig. S4 in Ref. [26]). First of all, one can notice the bottom of the Ti $3d$ band shifting gradually below the Fermi energy to form an expanding electron pocket at the M point due to the electron doping, which is consistent with the Fermi surface data shown in Fig. 1(c). The shift reaches to about 170 meV at its saturation of 0.5 ML. From above 0.10 ML, one can further notice a very peculiar W-shape dispersion of the Ti $3d$ band, deviating largely from the parabolic dispersion expected. This band has a strongly k_z-dependent spectral weight, which makes its center at the L point very weak (Fig. S1 in Ref. [26]). This is why the previous ARPES work [24] could not notice its W-shape dispersion (Fig. S1 in Ref. [26]). At a higher coverage above 0.3 ML, an additional band appears marginally occupied near the Fermi level. These two bands (green and red, called C^1_T and C^1_B, respectively) are attributed to the splitting of the contribution from Ti atoms of the first and the second layer as explained below. The previous ARPES and DFT study elucidated that the lowest Ti $3d$ (C^1) band is not actively involved in the CDW formation as a spectator-type band (Fig. 3) [25]. In contrast, the C^2 bands in higher energy participate in the CDW formation [25]. Thus, the CDW band gap must be defined between V and C^2 bands, which is experimentally not accessible since the C^2 band cannot be observed by ARPES. On the other hand, the valence band V shows a much smaller shift, a slightly upward shift and then downward, and an extra splitting above 0.25 ML (detailed discussion below). The strong renormalization and the different amounts of shifts in the lowest conduction band and the top valence band deviate largely from the conventional rigid shift of the bands due to the charge transfer from alkali metal adsorbates.

The peculiar band reconstruction observed is, however, well captured in the DFT calculation. Figure 3 shows the band dispersions calculated around the M point for the pristine CDW structure and for the system with K adatoms of 0.25 ML (one adatom per CDW unitcell). For the pristine $1T$-$TiSe_2$, the DFT calculation shows the multiple Se $4p$ valence bands, the spectator-type Ti $3d$ bands just above the Fermi energy, and the higher energy Ti $3d$ bands. Since the present structure

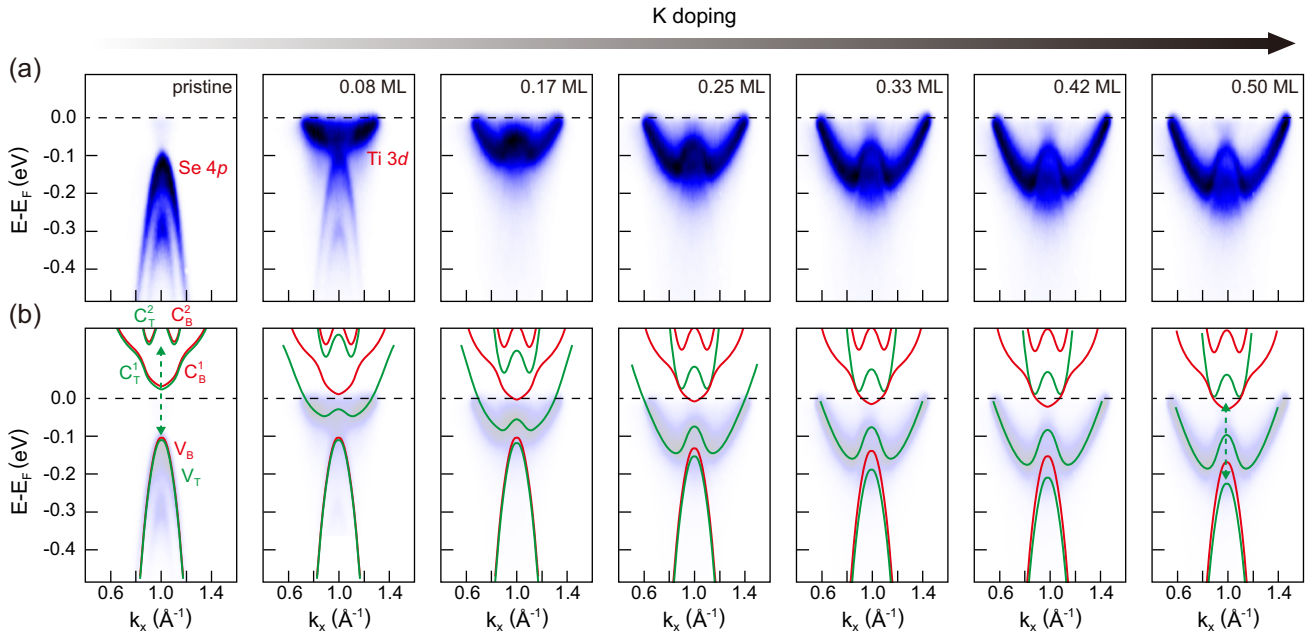

FIG. 2. (a) Evolution of the Ti 3*d* band and the Se 4*p* folded band at the M point upon increasing the K coverage. All spectra were measured at a temperature of 10 K with a horizontally polarized photon beam of 100 eV in energy. The schematics of the observed bands are overlayed on the measured spectral maps with reduced contrast in (b). The schematics of the unoccupied bands are from the DFT calculations with the correction of the band gap size (see the text for further explanation). Green and red bands originate from top and bottom layers, respectively. CDW band gap is indicated by dashed arrows.

model uses a double layer, all these bands are split due to the bonding-antibonding type interlayer interaction beyond the degeneracy of atomic orbitals. In this calculation, the CDW band gap is estimated to be about 220 meV. However, it was reported that DFT underestimates the band gap of this material, as usual for a gapped material [36]. As a result, the DFT calculation also underestimates the gap across the Fermi energy between the Se 4*p* and the spectator-type Ti 3*d* bands as 50 meV, which was measured to be 180 meV by ARPES. (Our schematic band dispersions in Fig. 2 are based on the present DFT calculation, but the band gap itself is enlarged to the experimental value for the pristine sample.)

For the system with K adsorbates, various K adsorption sites are compared with full relaxation of the surface structures and two sites, one on top of a Se atom (red-circled) and the other at the hollow (blue-circled) site, are found to energetically favored as shown in Fig. 1(a). The hollow site is the most stable [Fig. 1(e)], and the top site is the second-most stable with an energy difference of 1.7 meV. The migration barrier to adjacent sites is calculated to be about 83 meV and the other sites exhibit a much higher energy difference of at least 16.4 meV. We thus exclude the possibility of the thermal fluctuation between adsorption sites for the measurements at least at 10 K. The band dispersion at 0.25 ML was examined with the most favored adsorption sites occupied fully. For the topmost layer, one can observe the occupation of the W-shaped metallic band and the downward shift of the Se 4*p* bands. Note, however, that the shift of the Se 4*p* band is much smaller than that of the W-shaped band, indicating that it is not a rigid shift of the whole band structure. In this aspect, one can also observe that the splitting of the multiple Se 4*p* and Ti 3*d* bands increases. In order to systematically trace the evolution of the band structure upon the increase of the K coverage, we intentionally increase the separation between the K and the topmost Se layers from the fully optimized value at 0.25 ML. The atomic positions of the substrate are fixed at the optimized ones of 0.25 ML. Therefore, while the coverage itself is fixed in this series of calculations, the charge transfer interaction between the K adatom layer and the substrate is systematically controlled. As shown in Fig. 3(a), one can confirm that (i) the gradual occupation of the lowest Ti 3*d* band, (ii) the downward shift of the whole bands, (iii) the increased splitting of Se 4*p* (Ti 3*d*) branches, and (iv) the changes in the shape of the bands around Γ. Overall, these behaviors match reasonably with the experimental observations discussed above. As the most prominent observation, the gradual occupation and the change of the dispersion of the C_T^1 band into a W shape are well depicted. The origin of the gradual occupation of the W-shaped Ti 3*d* band is obviously the electron donation from K adatoms, which can be confirmed by the substantial K 4*s* contribution in the orbital decomposed band dispersions (Fig. S6 in Ref. [26]).

We also find that the increased splitting between the branches of Se 4*p* (Ti 3*d*) bands is mainly due to the increased difference between the bands of the first and the second layers since the electrons donated from K is well confined within the first layer [Figs. 1(e) and 3(b)–3(d)]. As a result, the top of the valence band comes mainly from the Se 4*p* band of the second layer, while the bottom of the conduction band manifold is due to the Ti 3*d* band of the first layer with K

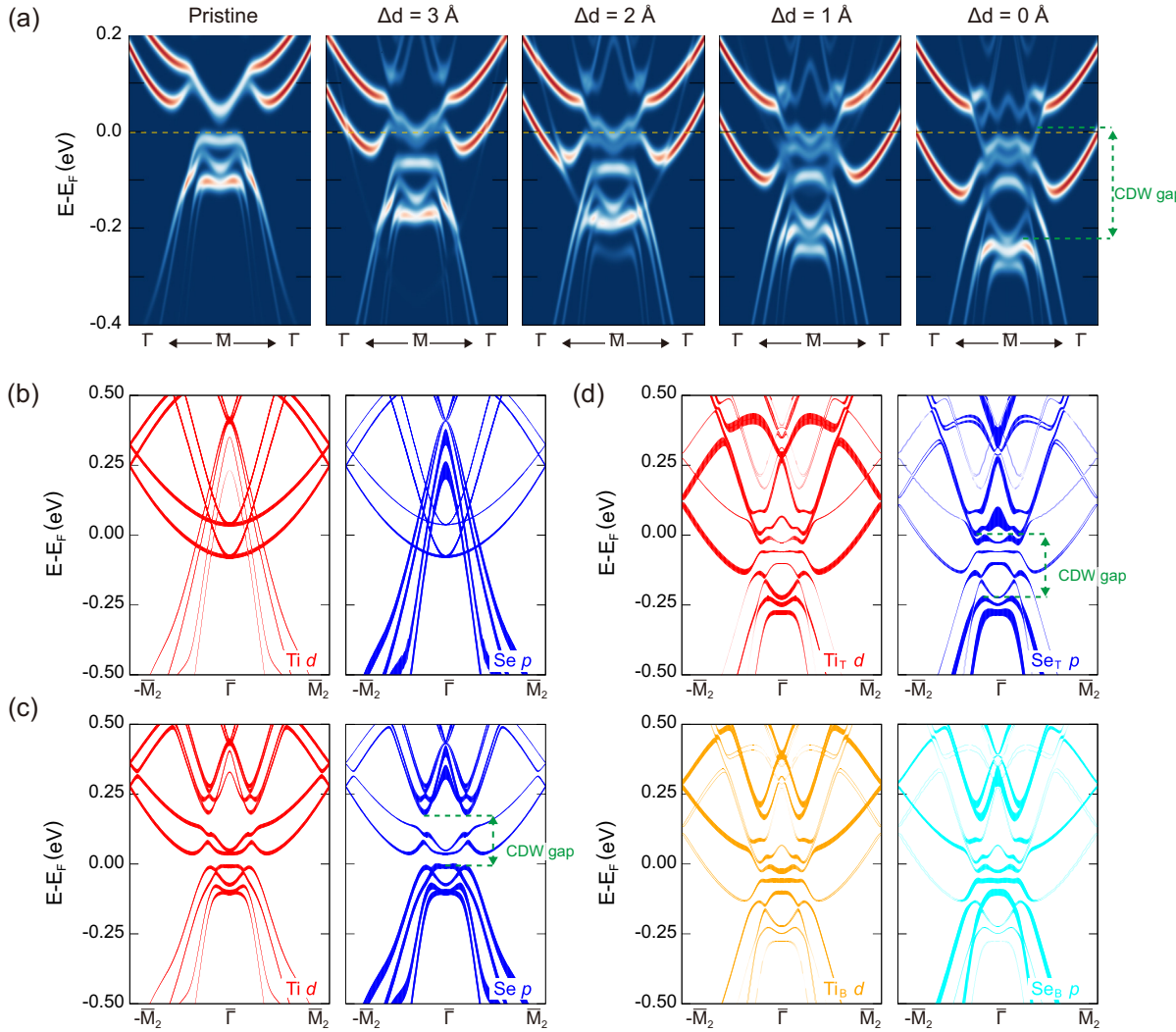

FIG. 3. (a) Unfolded band structure of pristine 2 × 2 CDW and doped 1T-TiSe$_2$ in the 1 × 1 brillouin zone (BZ) of 1T-TiSe$_2$. The Δd indicates the distance of the K atom from its optimized distance ($\Delta d = 0$ Å). All other structural parameters are fixed to the optimized values. Orbital-resolved band structures calculated for (b) the undistorted 1T-TiSe$_2$ folded into the 2 × 2 supercell, (c) the optimized 2 × 2 CDW structure, and (d) the 2 × 2 CDW structure optimized with 0.25 ML K. $\overline{M}_2$ denotes the M point of the 2 × 2 supercell BZ. In (d), the top (labeled by the subscript T) and the bottom layer (subscript S) bands are separately displayed in the top and the bottom pannel, respectively.

[Figs. 4(a) and 4(b)]. Note that the second layer band dispersion is largely preserved under the K adsorption [comparing the band dispersions of Figs. 3(c) and 3(d)]. Note also that the split bands in the pristine case are not layer resolved but correspond to the bonding-antibonding splitting of the two layers.

The above calculations show that the CDW band gap (the gap between the Se 4p bands and the upper Ti 3d bands) is almost intact in the first and the second layer. A consistent result was obtained with the lattice structure fully relaxed upon the change of the separation between the adlayer and the surface layer. The displacement of Ti atoms in the optimized structure with 0.25 ML is about half of that of the pristine CDW structure so that it enhances upon the increase of the separation (Fig. S5 in Ref. [26]). Nevertheless, the calculated band dispersion exhibits little difference from those with a fixed CDW structure. This is also consistent with the recent STM result which shows that the local CDW persists after the K adsorption [31]. This tells that the effect of the K adsorption and the subsequent electron doping has little effect on the existence of the CDW itself. This can be confirmed by the intensity of the Se 4p band folded into M by the CDW superstructure. As shown in Fig. 4(c), the Se 4p intensity at M exhibits no reduction up to about 0.2 ML. However, the CDW band gap cannot directly be measured in the ARPES experiment since the upper edge of the CDW band gap is not occupied; the marginally occupied band above 0.3 ML is assigned to the spectator Ti 3d band of the second layer (see Fig. S1 in Ref. [26]). One may find a hint of the CDW band gap variation in the shift of the Se 4p band. As mentioned above, the top of the Se 4p band initially moves upward and then shifts down and splits [Fig. 4(d)]. While the DFT calculation can explain the shift to a higher binding energy and the splitting, the initial upward shift cannot be explained.

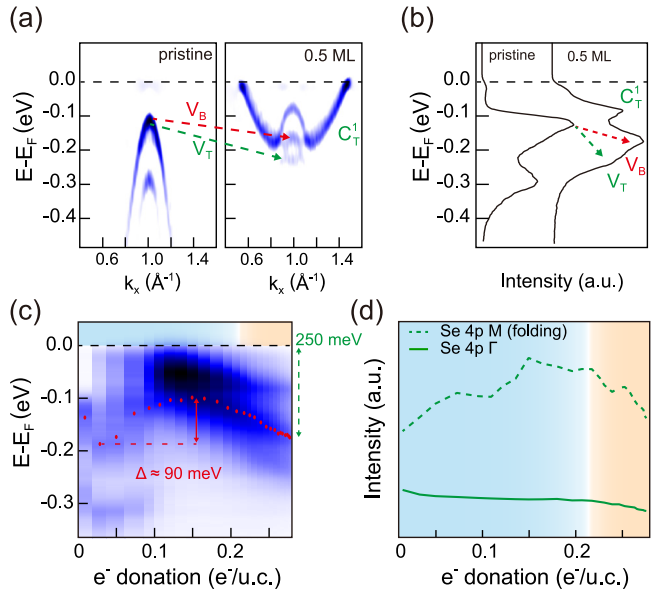

FIG. 4. (a) Second derivative ARPES spectra of pristine and 0.5 ML samples measured at $T = 10$ K. The splitting of Se $4p$ V band is indicated with red and green dashed lines. (b) Energy distribution curves at the M point of pristine and 0.5 ML cases. (c) Evolution of ARPES spectral intensity at the M point at T = 10 K as function of the K coverage (converted into the amount of electrons donated). Red dots indicate the location of V_B band, which exhibit an energy shift up to 90 meV. (d) Evolution of the intensity of the Se $4p$ band folded to the M point upon the increase of the amount of electrons donated as normalized by the intensity of the same band at Γ.

We may interpret this change as due to the change of the band gap [Fig. 5(a)], which is not depicted in the current DFT calculation. Evidence of this interpretation is that the two Se $4p$ bands shift to opposite directions as shown in Fig. 5(b). That is, only the top branch of the valence band shifts in a different way, which reflects the band gap renormalization. The other evidence of the band shape change against a rigid shift can be found in the momentum distribution curves of the ARPES spectral maps as shown in Fig. 5(c). The width of the V band at a binding energy of 0.5 eV decreases slightly after the initial K deposition. A rigid shifts must yield an opposite change but the band gap decrease would produce the narrowing of the band width in momentum as shown in Fig. 5(d). The size of the initial upward shift is, however, not quantitatively determined since the initial bonding-antibonding hybridization of the bands of the first and the second layer is not consistent after K adsorption, which breaks the layer symmetry. The size of the upward shift is about 90 meV at most and when the band gap change is symmetric with respect to the Fermi energy, the change of the band gap should be less than 180 meV. This part of the gap change can, thus, be due to the change of many-body interactions beyond the local density approximation, which include the excitonic interaction as a part [36]. It is natural to expect the reduction of many-body interactions due to the screening by metallic electrons. However, the remaining CDW gap is larger than 250 meV, and this is much larger than the reduced part, which is less than 180 meV as explained above. Thus, the electron correlation effect beyond DFT accounts for less than a half of the total band gap and the CDW itself is robust against the changes in such electronic many-body interactions. Since the excitonic interaction is only a part of electronic many-body effects [36], the excitonic contribution may be smaller than 180 meV. In any case, the present result indicates that the electron many-body interaction or the excitonic interaction is not critical in the CDW formation. In this work, we did not consider the CDW pinning by adsorbates. However, the pinning effect must be not so substantial since the K adsorbate does not enhance the lattice displacement (Fig. S5 in Ref. [26]). Even when the lattice is locally pinned into the 2×2 structure, excitons and the excitonic band gap would be suppressed by metallic electrons doped. This case can be denied by the present result. The excitonic gap is expected to be completely suppressed around the metallic electron density of 0.16 $e^-/u.c.$, which corresponds to the coverage around 0.18 ML in the present work [19,37].

The present conclusion is consistent with the recent electron-energy loss spectroscopy result, which ruled out the plasmon softening in the transition. On the other hand, the present conclusion is not consistent with the very recent ARPES work for the K adsorption on the same system [24]. We note that this ARPES experiment misinterpreted the W-shape C_T^1 band as a parabolic band and the occupation of another Ti $3d$ band due to the strong photon-energy dependence unnoticed. This interpretation was then plugged into

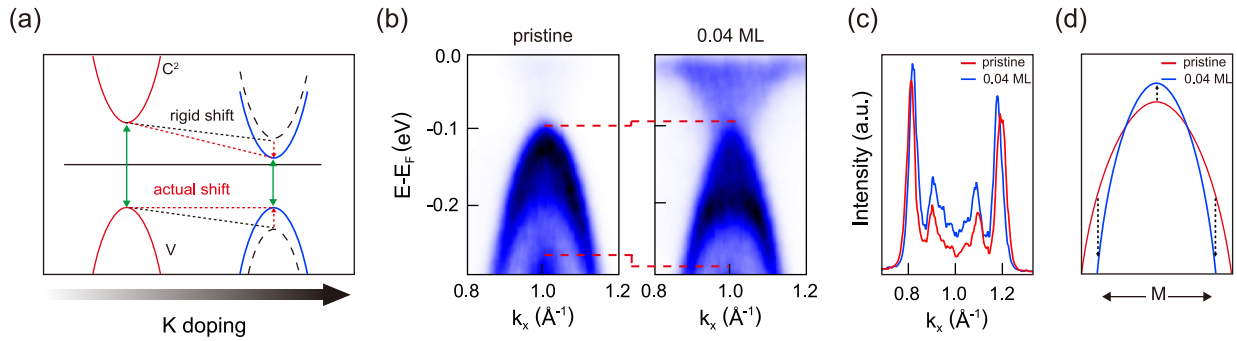

FIG. 5. (a) Schematics of the shifts of the CDW related bands (V and C^2) upon the K adsorption. (b) ARPES measurements around the M point of the pristine 1T-$TiSe_2$ and that with K adsorbates of 0.04 ML. The shift of the valence band top is indicated with red dashed lines. (c) Momentum distribution curves at $E - E_F = -0.5$ eV of the spectra shown in (b). (d) Schematics of the change of the valence band (V).

the excitonic model to estimate the band gap, which produced a substantial reduction of the excitonic band gap with only a minor part of the gap (the band gap due to the periodic lattice distortion within this interpretation) remaining. Our measurements and calculation do not support the collapse of the major part of the band gap and do not provide conclusive evidence of the excitonic origin of the band gap reduced. Another recent work [38] reported that the generation of Se vacancies donates electrons into the system and the CDW is suppressed as noticed by the suppressed intensity of the Se $4p$ folded band. However, even in that case, the CDW band gap itself as defined in the present and the recent works [24,25] is not closed at all. In general, the fact that the structure and the band gap of CDW are preserved upon the metallization of the system is not compatible with the excitonic or correlation origin of CDW. However, this can be explained by the Jahn-Teller-type CDW mechanism, where the energy lowering by the splitting of the band due to the electron-phonon coupling is crucial.

IV. CONCLUSIONS

In summary, we trace using ARPES the evolution of the band dispersions of $1T$-$TiSe_2$ in its CDW state during the continuous K deposition. We find the strong band reconstruction by the K adsorption, which reaches well beyond the rigid shift due to the charge tranfer or electron doping from alkali metal adsorbates. Firstly, the electron transfer is highly band-selective to fill the lowest Ti $3d$ band, which is not relevant to the formation of CDW. Secondly, the electron transfer is well localized to the topmost layer to split the bands from the first and the second layer. Thirdly, the major part of the CDW band gap and the CDW amplitude do not change significantly irrespective of the strong electron doping. These results indicate the robustness of the CDW in the present system against the electron doping and is not compatible with the existence of the strong excitonic interaction for the CDW formation. Instead, the present observation is largely in line with the band Jahn-Teller mechanism of the CDW formation. The band- and layer-selective doping has wide implication for electronic transitions in van der Waals systems with multiple bands. In particular, the dichotomy of the metallic electrons and the electronic transition of CDW in the present system suggests that the superconductivity and the CDW are not necessarily competitive or entangled.

ACKNOWLEDGMENTS

We thank J. Denlinger for supporting the ARPES experiment in the ALS. This work was supported by the Institute for Basic Science (Grant No. IBS-R014-D1). K.-H.J. is supported by the Institute for Basic Science (Grant No. IBS-R014-Y1). The ALS is supported by the US Department of Energy, Office of Sciences, under contract No. DE-AC02-05CH11231.

[1] K. Novoselov, O. A. Mishchenko, O. A. Carvalho, and A. Castro Neto, Science **353**, aac9439 (2016).
[2] P. Fazekas and E. Tosatti, Philosophical Magazine B **39**, 229 (1979).
[3] K. T. Law and P. A. Lee, Proc. Natl. Acad. Sci. USA **114**, 6996 (2017).
[4] T. E. Kidd, T. Miller, M. Y. Chou, and T.-C. Chiang, Phys. Rev. Lett. **88**, 226402 (2002).
[5] H. Cercellier, C. Monney, F. Clerc, C. Battaglia, L. Despont, M. Garnier, H. Beck, P. Aebi, L. Patthey, H. Berger, and L. Forró, Phys. Rev. Lett. **99**, 146403 (2007).
[6] C. Monney, C. Battaglia, H. Cercellier, P. Aebi, and H. Beck, Phys. Rev. Lett. **106**, 106404 (2011).
[7] C. Monney, H. Cercellier, F. Clerc, C. Battaglia, E. F. Schwier, C. Didiot, M. G. Garnier, H. Beck, P. Aebi, H. Berger, L. Forró, and L. Patthey, Phys. Rev. B **79**, 045116 (2009).
[8] B. Sipos, A. F. Kusmartseva, A. Akrap, H. Berger, L. Forró, and E. Tutiš, Nat. Mater. **7**, 960 (2008).
[9] R. Ang, Y. Tanaka, E. Ieki, K. Nakayama, T. Sato, L. J. Li, W. J. Lu, Y. P. Sun, and T. Takahashi, Phys. Rev. Lett. **109**, 176403 (2012).
[10] P. Xu, J. O. Piatek, P.-H. Lin, B. Sipos, H. Berger, L. Forró, H. M. Rønnow, and M. Grioni, Phys. Rev. B **81**, 172503 (2010).
[11] E. Morosan, H. W. Zandbergen, B. S. Dennis, J. W. G. Bos, Y. Onose, T. Klimczuk, A. P. Ramirez, N. P. Ong, and R. J. Cava, Nat. Phys. **2**, 544 (2006).
[12] A. F. Kusmartseva, B. Sipos, H. Berger, L. Forró, and E. Tutiš, Phys. Rev. Lett. **103**, 236401 (2009).
[13] L. J. Li, E. C. T. O'Farrell, K. P. Loh, G. Eda, B. Özyilmaz, and A. H. Castro Neto, Nature (London) **529**, 185 (2016).
[14] F. J. Di Salvo, D. E. Moncton, and J. V. Waszczak, Phys. Rev. B **14**, 4321 (1976).
[15] A. Zunger and A. J. Freeman, Phys. Rev. B **17**, 1839 (1978).
[16] H. P. Hughes, J. Phys. C **10**, L319 (1977).
[17] M. H. Whangbo and E. Canadell, J. Am. Chem. Soc. **114**, 9587 (1992).
[18] K. Rossnagel, L. Kipp, and M. Skibowski, Phys. Rev. B **65**, 235101 (2002).
[19] M. Porer, U. Leierseder, J.-M. Ménard, H. Dachraoui, L. Mouchliadis, I. Perakis, U. Heinzmann, J. Demsar, K. Rossnagel, and R. Huber, Nat. Mater. **13**, 857 (2014).
[20] A. Wegner, J. Zhao, J. Li, J. Yang, A. A. Anikin, G. Karapetrov, K. Esfarjani, D. Louca, and U. Chatterjee, Phys. Rev. B **101**, 195145 (2020).
[21] A. Kogar, M. S. Rak, S. Vig, A. A. Husain, F. Flicker, Y. I. Joe, L. Venema, G. J. MacDougall, T. C. Chiang, E. Fradkin *et al.*, Science **358**, 1314 (2017).
[22] J. M. Bok, J. Hwang, and H.-Y. Choi, Phys. Rev. B **103**, 205108 (2021).
[23] Z. Lin, C. Wang, A. Balassis, J. P. Echeverry, A. S. Vasenko, V. M. Silkin, E. V. Chulkov, Y. Shi, J. Zhang, J. Guo, and X. Zhu, Phys. Rev. Lett. **129**, 187601 (2022).
[24] T. Jaouen, A. Pulkkinen, M. Rumo, G. Kremer, B. Salzmann, C. W. Nicholson, M.-L. Mottas, E. Giannini, S. Tricot, P. Schieffer *et al.*, Phys. Rev. Lett. **130**, 226401 (2023).

[25] M. D. Watson, O. J. Clark, F. Mazzola, I. Marković, V. Sunko, T. K. Kim, K. Rossnagel, and P. D. C. King, Phys. Rev. Lett. **122**, 076404 (2019).
[26] See Supplemental Material at http://link.aps.org/supplemental/10.1103/PhysRevB.109.125117 for detailed comparison with the previous ARPES results and extended DFT results.
[27] G. Kresse and J. Furthmüller, Phys. Rev. B **54**, 11169 (1996).
[28] J. P. Perdew, K. Burke, and M. Ernzerhof, Phys. Rev. Lett. **77**, 3865 (1996).
[29] A. Subedi, Phys. Rev. Mater. **6**, 014602 (2022).
[30] C. Ramırez and W. Schattke, Surf. Sci. **482-485**, 424 (2001).
[31] K.-W. Zhang, C.-L. Yang, B. Lei, P. Lu, X.-B. Li, Z.-Y. Jia, Y.-H. Song, J. Sun, X. Chen, J.-X. Li, and S.-C. Li, Sci. Bull. **63**, 426 (2018).
[32] J. Luttinger, Phys. Rev. **119**, 1153 (1960).
[33] T. Rohwer, S. Hellmann, M. Wiesenmayer, C. Sohrt, A. Stange, B. Slomski, A. Carr, Y. Liu, L. M. Avila, M. Kalläne, S. Mathias, L. Kipp, K. Rossnagel, and M. Bauer, Nature (London) **471**, 490 (2011).
[34] P. Chen, Y.-H. Chan, X.-Y. Fang, S.-K. Mo, Z. Hussain, A.-V. Fedorov, M. Chou, and T.-C. Chiang, Sci. Rep. **6**, 37910 (2016).
[35] D. Qian, D. Hsieh, L. Wray, E. Morosan, N. L. Wang, Y. Xia, R. J. Cava, and M. Z. Hasan, Phys. Rev. Lett. **98**, 117007 (2007).
[36] M. Cazzaniga, H. Cercellier, M. Holzmann, C. Monney, P. Aebi, G. Onida, and V. Olevano, Phys. Rev. B **85**, 195111 (2012).
[37] Y. Cheng, A. Zong, J. Li, W. Xia, S. Duan, W. Zhao, Y. Li, F. Qi, J. Wu, L. Zhao, P. Zhu, X. Zou, T. Jiang, Y. Guo, L. Yang, D. Qian, W. Zhang, A. Kogar, M. W. Zuerch, D. Xiang, and J. Zhang, Nat. Commun. **13**, 963 (2022).
[38] T. Jia, S. N. Rebec, S. Tang, K. Xu, H. M. Sohail, M. Hashimoto, D. Lu, R. G. Moore, and Z.-X. Shen, 2D Mater. **6**, 011008 (2018).